

$^{12}\text{C}/^{13}\text{C}$ ratio in planetary nebulae from the IUE archives

R.H. Rubin^{1,2}

G.J. Ferland³

E.E. Chollet¹

R. Horstmeier¹

rubin@cygnus.arc.nasa.gov; gary@pa.uky.edu

ABSTRACT

We investigated the abundance ratio of $^{12}\text{C}/^{13}\text{C}$ in planetary nebulae by examining emission lines arising from C III $2s2p\ ^3P_{2,1,0} \rightarrow 2s^2\ ^1S_0$. Spectra were retrieved from the International Ultraviolet Explorer archives, and multiple spectra of the same object were coadded to achieve improved signal-to-noise. The ^{13}C hyperfine structure line at 1909.6 Å was detected in NGC 2440. The $^{12}\text{C}/^{13}\text{C}$ ratio was found to be $\sim 4.4 \pm 1.2$. In all other objects, we provide an upper limit for the flux of the 1910 Å line. For 23 of these sources, a lower limit for the $^{12}\text{C}/^{13}\text{C}$ ratio was established. The impact on our current understanding of stellar evolution is discussed.

The resulting high signal-to-noise C III spectrum helps constrain the atomic physics of the line formation process. Some objects have the measured 1907/1909 flux ratio outside the low-electron density theoretical limit for ^{12}C . A mixture of ^{13}C with ^{12}C helps to close the gap somewhat. Nevertheless, some observed 1907/1909 flux ratios still appear too high to conform to the presently predicted limits. It is shown that this limit, as well as the 1910/1909 flux ratio, are predominantly influenced by using the standard partitioning among the collision strengths for the multiplet $^1S_0\text{--}^3P_J$ according to the statistical weights. A detailed calculation for the fine structure collision strengths between these individual levels would be valuable.

Subject headings: Atomic processes — planetary nebulae: abundances, general, individual (NGC 2440) — stars: abundances, AGB and post-AGB

¹NASA/Ames Research Center, Moffett Field, CA 94035-1000.

²Orion Enterprises, M.S. 245-6, Moffett Field, CA 94035-1000

³University of Kentucky, Department of Physics and Astronomy, Lexington, KY 40506.

1. Introduction

The relative abundances of ^{12}C and ^{13}C in evolved stars present a strong challenge to our current understanding of stellar nucleosynthesis. A growing body of observational evidence suggests that standard stellar models greatly overestimate the ratio of ^{12}C to ^{13}C on the red giant branch (RGB) and later evolution. In a careful study of the literature, Charbonnel & do Nascimento (1998) have shown that a full 96% of evolved stars exhibit a $^{12}\text{C}/^{13}\text{C}$ ratio below 15, considerably lower than models predict ($^{12}\text{C}/^{13}\text{C}$ between 20 – 30). On the other hand, cool bottom processing (CBP), which employs a deep mixing mechanism below the standard convective envelope during the red giant phase (Sackmann & Boothroyd 1999), predicts $^{12}\text{C}/^{13}\text{C}$ ratios ≤ 20 for low-mass post-RGB stars (Boothroyd & Sackmann 1999). Using millimeter wave observations of ^{12}CO and ^{13}CO , Palla et al. (2000) found several examples of planetary nebulae (PNs) with small $^{12}\text{C}/^{13}\text{C}$ ratios, as low as 9 for NGC 7293. Balser et al. (2002) in a similar study measured ^{12}CO and ^{13}CO in molecular clouds associated with PNs. They found the range of $^{12}\text{C}/^{13}\text{C}$ from 2.2–31 in 9 PNs. The extreme low value 2.2 ± 0.03 was found for the PN M1–16. Developing another approach to obtaining these abundance ratios is very valuable to corroborate these low values.

Clegg (1985) pointed out that the $^{12}\text{C}/^{13}\text{C}$ ratio could be determined using an extremely weak C III ^{13}C line at 1909.597 Å. This line is a hyperfine induced transition that arises from $2s2p\ ^3P_0 \rightarrow 2s^2\ ^1S_0$, which is strictly forbidden in ^{12}C . By comparing the flux of this line to the nearby bright C III lines $2s2p\ ^3P_{2,1} \rightarrow 2s^2\ ^1S_0$ at 1906.683 Å and 1908.734 Å respectively, one can find the $^{12}\text{C}/^{13}\text{C}$ ratio. Using the Hubble Space Telescope (HST), Clegg et al. (1997) found a ratio of 15 ± 3 in NGC 3918 and 21 ± 11 in SMC N2, as well as a very marginal 7_{-3}^{+14} for LMC N122. Palla et al. (2002), also using HST, reported a non-detection in NGC 3242, showing $^{12}\text{C}/^{13}\text{C} \geq 38$.

When studying faint lines in extended sources, the light gathering power of the instrument is extremely important. The large IUE aperture, an $\sim 20'' \times \sim 10''$ ‘rounded rectangle’ (also described as an oval or race-track pattern), allowed a high throughput for extended objects like PNs. The extensive archival database and New Spectral Image Processing System (NEWSIPS) allow us to effectively study the 1909.597 Å ^{13}C line with IUE. Using these data, coadding multiple spectra when available to get a higher signal-to-noise ratio (S/N), we attempt to measure or provide upper limits for the flux of this line. In conjunction with our measurements of fluxes in the adjacent “main” lines, we derive or set limits for the $^{12}\text{C}/^{13}\text{C}$ ratio in most of the sample of PNs.

In section 2, we discuss the IUE database and our flux measurements. The analysis tools to interpret the observations are introduced in section 3, with the population rate equations. In section 4, the flux ratios are analyzed in terms of the $^{12}\text{C}/^{13}\text{C}$ ratio and the electron

density (N_e). Section 5 contains a discussion and conclusions.

2. IUE Observations

The data were obtained from the IUE archives. For most sources, only short wavelength prime (SWP) camera spectra with the large aperture were used, because the long wavelength spectra taken with both the prime camera (LWP) and redundant camera (LWR) are much noisier at this wavelength. The spectral resolution of high dispersion SWP, LWP, or LWR spectra at these wavelengths is ~ 0.2 Å, sufficient to separate the weak ^{13}C line from the bright line at 1908.7 Å.

We included all promising PNs observed with high dispersion in the large aperture. Multiple observations of the same object were coadded point by point, weighted by the inverse of the total noise in the continuum, to improve the S/N, using our own analysis program. We note that the inverse noise and exposure time are not linearly related in IUE spectra. Figure 1 shows a plot of inverse noise vs. integration time for NGC 3918 SWP spectra. Though the data quality, as gauged by inverse noise, generally improves with increased time, the quality is not a linear relation of either exposure time or the square root of the exposure time. The IUE on-line “Frequently Asked Questions” (<http://archive.stsci.edu/cgi-bin/faq.cgi?mission=IUE#40>) recommends inverse noise weighting, and our data show that weighting by the inverse noise generates better S/N than weighting by the time or by the square root of the time.

The ISAP¹ routine Line Fit was used to fit a three-component Gaussian to the three lines of the C III multiplet in order to determine the line fluxes or to set an upper limit when a line was not detected. The number of free parameters were limited by constraining the full width half maximum (FWHM) to be that of the 1907 Å line. Only one degree of freedom in the determination of wavelength was allowed by requiring the fit to conform to the known $\Delta\lambda_{vac}$ between the transitions – that is an offset of 2.051 and 2.914 Å for the 1909 and 1910 lines relative to the 1906.683 Å line. We use a quadratic continuum fit to the line-free data. Most of the IUE spectra that we found useful are SWP spectra. For fitting the continuum baseline in these, we avoid the data points at lower wavelength than the 1907 Å line where there is an echelle interorder “splice” (at ~ 1905.4) and the fluctuations in the continuum intensity become much larger than those on the red side.

¹ISO Spectral Analysis Package (ISAP) is a joint development by the LWS and SWS Instrument Teams and Data Centers. Contributing institutes are CESR, IAS, IPAC, MPE, RAL, & SRON.

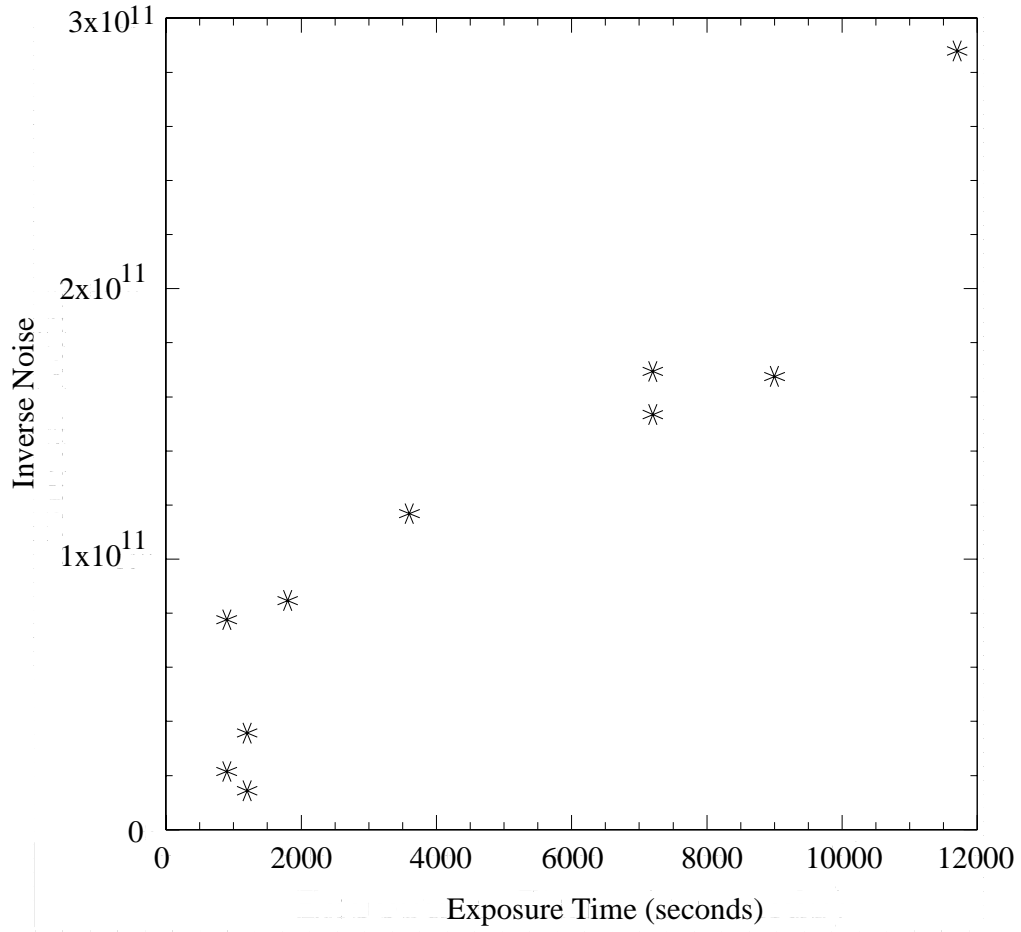


Fig. 1.— The inverse noise (the reciprocal of the sum of noise points from $\sim 1910.5\text{--}1920 \text{ \AA}$) versus the exposure time for the various SWP high dispersion, large aperture IUE spectra of NGC 3918. Units in the ordinate are relative; a larger value indicates less noisy data.

We used both Gaussian-fitting and direct integration routines to measure the net line flux above the continuum. Because the filled large aperture introduced a spectral impurity into the spectrograph, the line profiles have flatter tops and less extended bases (e.g., are more “trapezoidal”) than the Gaussian fits. For this reason and because some of the sources have lines that depart in other ways from Gaussian, we prefer to use the direct integration routines (the moment option in ISAP) to measure the line flux. We also confirmed our line flux results using IRAF² splot with the e-option for direct integration.

The root-mean-square (rms) fluctuations in the continuum flux were determined from a region clear of lines and obvious spikes longward of 1910 Å and the FWHM determined from the 1906.7 Å line. From this, we determine the value 3σ , which is our threshold for judging a flux measurement a detection or not. This 3σ value is also used to set upper limits on the flux for the non-detections. The results of our measurements are presented in Table 1. Column 1 has the source name; columns 2 and 3 the J2000 positions; columns 4, 6, and 8 have the line flux measurements $F(1906.7)$, $F(1908.7)$, and $F(1909.6)$ in $\text{erg cm}^{-2} \text{s}^{-1}$. Column 5 has the 1σ uncertainty associated with each of the line fluxes while column 7 is 3 times this value in order to judge whether or not the hyperfine line has been detected. The FWHM from the Gaussian fit of the coadded, unsaturated spectra are in column 9. The entries in the remaining columns are quantities derived from these data and will be discussed later.

For many of the sources, there is a second line in Table 1 where more IUE spectra were coadded with those used to produce the first-line results (with *only unsaturated data*). These added spectra are saturated in either the 1907 or 1909 lines. Because of the limited dynamic range of IUE, long exposures, particularly with the SWP camera, of bright PNs will readily saturate (overexpose) these strong C III lines. However, there is not a saturation issue with the 1910 line and adjacent continuum. Using these additional data, we are able to test if there are now any statistically significant detections of the 1910 line by comparing $F(1909.6)$ with the 3σ uncertainty, which is generally smaller than the entry on line 1. Although the resulting flux and FWHM in the main lines are not reliable, we are able to use these lines as a fiducial wavelength indicator only to fit the data in the vicinity of the 1910 Å line with a single Gaussian that has a FWHM assumed to be the same as on line 1. As will be discussed (§4.2), the only object with a significant detection of the 1910 line is NGC 2440. Even with the additional data entered on line 2, we found no other significant detections of this line.

²IRAF is distributed by NOAO, which is operated by AURA, under cooperative agreement with NSF.

Table 1. C III Line Fluxes and Derived Parameters

Object	RA	J2000	DEC	F(1906.7)	1σ error	F(1908.7)	3σ	F(1909.6)	FWHM	1907/1909	N_e cm $^{-3}$	r ($^{12}\text{C}/^{13}\text{C}$)
PN G108.2-76.1	00 37 16.0		-13 43 00	2.79E-12	3.42E-14	1.93E-12	1.03E-13	-5.24E-14	0.3670	1.45	1580–2120	>3
					2.04E-14		6.11E-14	3.00E-14				
IC 351	03 47 32.9		+35 02 48	1.71E-12	7.91E-14	1.40E-12	2.37E-13	3.81E-14	0.2955	1.22	8360	—
IC 2003	03 56 22.0		+33 52 28	4.97E-12	8.87E-14	3.40E-12	2.66E-13	-1.26E-13	0.4451	1.46	1170–1950	>1.8
					4.63E-14		1.39E-13	-6.39E-14				
NGC 1535	04 14 15.9		-12 44 21	7.99E-12	1.06E-13	5.97E-12	3.17E-13	-1.40E-13	0.5714	1.34	4550–5140	>1.9
					6.35E-14		1.91E-13	-6.00E-15				
IC 418	05 27 28.2		-12 41 50	1.59E-11	9.57E-14	1.42E-11	2.87E-13	1.61E-13	0.3658	1.12	12300–12600	>3.4
					4.06E-14		1.22E-13	2.70E-14				
NGC 2022	05 42 06.2		+09 05 10	3.56E-12	6.09E-14	2.40E-12	1.83E-13	-5.99E-14	0.6721	1.48	660–1400	>2.1
IC 2149	05 56 24.0		+46 06 15	2.96E-12	3.69E-14	2.26E-12	1.11E-13	2.12E-14	0.3213	1.31	5400–5960	>1.9
					2.80E-14		8.39E-14	-5.52E-15				
IC 2165	06 21 42.6		-12 59 10	1.04E-11	2.05E-13	5.80E-12	6.14E-13	-9.74E-14	0.4423	1.79	out of range	
					4.73E-14		1.42E-13	-6.95E-14				
NGC 2346	07 09 22.5		-00 48 24	7.01E-13	3.29E-14	4.95E-13	9.87E-14	2.66E-14	0.4853	1.42	2360	—
					3.42E-14		1.02E-13	1.67E-14				
NGC 2440	07 41 55.4		-18 12 33	2.24E-11	1.47E-13	1.57E-11	4.41E-13	5.94E-13	0.5399	1.427	2460	4.4±1.2
PN G264.4-12.7	07 47 20.4		-51 15 05	7.94E-13	1.92E-14	6.15E-13	5.76E-14	3.01E-14	0.2851	1.29	6000–7080	>0.43
IC 2448	09 07 06.6		-69 56 29	8.06E-12	1.29E-13	5.00E-12	3.87E-13	-1.06E-13	0.3831	1.61	out of range	
					3.10E-14		9.30E-14	5.33E-14				
NGC 2867	09 21 25.5		-58 18 35	2.42E-11	1.26E-13	1.87E-11	3.77E-13	9.22E-14	0.4567	1.29	5900–6130	>5.9
					9.29E-14		2.79E-13	4.31E-14				
NGC 3132	10 07 01.8		-40 26 11	1.71E-12	5.43E-13	1.08E-12	1.63E-12	-1.33E-13	0.6262	1.58	out of range	
					2.21E-13		6.63E-13	-1.24E-13				
NGC 3211	10 17 50.4		-62 40 12	7.94E-12	7.74E-14	6.04E-12	2.32E-13	2.24E-14	0.4637	1.31	5250–5680	>2.8
NGC 3242	10 24 46.1		-18 38 33	4.71E-11	2.51E-13	3.15E-11	5.31E-13	5.13E-14	0.5662	1.50	370–530	>14.5
					1.00E-13		3.00E-13	1.28E-13				
NGC 3918	11 50 17.2		-57 10 53	6.94E-11	2.16E-13	5.48E-11	6.48E-13	1.64E-13	0.4605	1.27	6810–6950	>9.9
					7.69E-14		2.31E-13	1.51E-13				
NGC 4361	12 24 30.7		-18 47 06	1.62E-12	6.75E-14	1.07E-12	2.02E-13	-6.51E-14	0.6478	1.51	out of range	
IC 3568	12 33 06.9		+82 33 49	5.14E-12	2.83E-13	2.96E-12	8.49E-13	5.27E-14	0.3498	1.74	out of range	
					3.46E-14		1.04E-13	4.53E-14				
NGC 5189	13 33 31.7		-65 58 23	3.77E-13	4.60E-14	3.00E-13	1.38E-13	-6.37E-14	0.6241	1.26	7120	—
NGC 5315	13 53 55.2		-66 30 52	1.08E-12	3.64E-14	1.90E-12	1.09E-13	1.06E-13	0.5320	0.57	58500	—
PN G342.1+27.5	15 22 19.3		-23 27 46	1.06E-11	7.06E-14	7.25E-12	2.12E-13	-4.57E-14	0.4228	1.46	1170–1470	>6.9

Table 1—Continued

Object	RA	J2000	DEC	F(1906.7)	1σ error	F(1908.7)	3σ	F(1909.6)	FWHM	1907/1909	N_e cm $^{-3}$	r ($^{12}\text{C}/^{13}\text{C}$)
IC 4593	16 11 44.5		+12 04 17	8.32E-13	4.29E-14	4.44E-13	1.29E-13	-1.08E-14	0.3637	1.87	out of range	
					4.07E-14		1.22E-13	-9.61E-15				
NGC 6210	16 44 29.5		+23 48 00	6.74E-12	5.65E-14	5.28E-12	1.69E-13	1.53E-13	0.4977	1.28	6450–6820	>3.1
					3.50E-14		1.05E-13	8.69E-14				
IC 4634	17 01 33.7		-21 49 31	8.28E-13	4.42E-14	6.57E-13	1.33E-13	-3.87E-14	0.4759	1.26	7010	—
NGC 6302	17 13 44.4		-37 06 11	4.60E-13	3.24E-14	3.69E-13	9.72E-14	1.64E-14	0.4363	1.25	7450	—
					3.57E-14		1.07E-13	8.36E-15				
PN G345.2-08.8	17 45 35.3		-46 05 23	1.34E-12	4.07E-14	1.06E-12	1.22E-13	-7.79E-17	0.3101	1.26	6880–8240	>0.08
					5.09E-14		1.53E-13	-1.31E-14				
NGC 6543	17 58 33.4		+66 37 60	9.25E-12	1.21E-13	7.38E-12	3.64E-13	-6.68E-14	0.4973	1.25	7250–7830	>1.5
					4.81E-14		1.44E-13	-1.97E-14				
NGC 6572	18 12 06.4		+06 51 13	1.37E-11	1.07E-13	1.47E-11	3.20E-13	-1.46E-13	0.3302	0.93	21900–22200	>1.7
					2.23E-14		6.68E-14	6.38E-14				
NGC 6644	18 32 34.7		-25 07 44	1.13E-11	2.60E-13	8.13E-12	7.80E-13	-4.17E-13	0.2668	1.39	3060–4080	>0.82
					4.64E-14		1.39E-13	-5.36E-14				
IC 1297	19 17 22.8		-39 36 46	4.43E-12	1.12E-13	3.47E-12	3.35E-13	-2.14E-13	0.4832	1.28	6450–7580	>0.33
NGC 6818	19 43 58.3		-14 09 09	1.09E-11	2.81E-13	6.29E-12	8.42E-13	-6.23E-13	0.5499	1.73	out of range	—
					4.04E-14		1.21E-13	-3.31E-15				
NGC 6826	19 44 48.2		+50 31 30	1.15E-11	1.34E-13	8.21E-12	4.05E-13	-3.86E-14	0.5048	1.40	2760–3280	>2.8
					9.47E-14		2.84E-13	4.56E-14				
NGC 6853	19 59 36.2		+22 43 01	1.69E-12	5.09E-14	1.19E-12	1.53E-13	-6.70E-14	0.6093	1.42	2250–3580	>0.46
NGC 6891	20 15 08.9		+12 42 17	2.40E-12	3.81E-14	1.73E-12	1.14E-13	1.21E-14	0.3325	1.39	3140–3840	>1.7
					4.02E-14		1.21E-13	-3.20E-14				
NGC 6905	20 22 22.9		+20 06 16	2.07E-12	6.85E-14	1.38E-12	2.06E-13	-1.46E-13	0.9453	1.50	250	—
NGC 7009	21 04 10.8		-11 21 49	1.49E-11	7.09E-14	1.22E-11	2.13E-13	1.92E-13	0.4601	1.22	8360–8570	>5.6
					9.99E-14		3.00E-13	2.34E-13				
NGC 7027	21 07 01.6		+42 14 10	3.64E-12	1.39E-13	4.88E-12	4.16E-13	2.07E-13	0.3556	0.75	36200	—
					5.90E-14		1.77E-13	1.36E-13				
PN G086.5-08.8	21 33 08.0		+39 39 02	2.38E-12	4.70E-14	1.51E-12	1.41E-13	-4.04E-14	0.6668	1.58	out of range	
					5.35E-14		1.61E-13	-3.49E-14				
IC 5217	22 23 55.8		+50 57 60	8.79E-13	5.37E-14	6.66E-13	1.61E-13	1.01E-14	0.3017	1.32	5090	—
NGC 7662	23 25 54.0		+42 32 06	4.55E-11	2.15E-13	3.53E-11	6.44E-13	-2.49E-14	0.5772	1.29	6060–6270	>6.5
					8.78E-14		2.63E-13	4.84E-14				

3. Rate Equations for the Level Populations

In order to interpret the observational data, we solve the C III statistical equilibrium equations for the populations of the 4 lowest-lying energy levels, numbered 1–4. These are $2s^2\ ^1S_0$, $2s2p\ ^3P_0$, $2s2p\ ^3P_1$, and $2s2p\ ^3P_2$. For this, the effective collision strengths (Υ values) and transition probabilities (A-values) listed in Table 2 are used. Note the important distinction for A_{21} between ^{12}C and ^{13}C . This is the sole quantity that is different and is the crucial factor in providing different results when solving the rate equations for the level populations. The effective collision strengths for transitions between the 3P_J levels are available for the electron temperature (T_e) = 5000, 10000, 15000, and 20000 K (Keenan et al. 1992). We use these same temperatures in Table 2, adding the recent data for 1S_0 – 3P_J (Mitnik et al. 2003 and Don Griffin, private communication). Then, following standard procedure, their value is partitioned among the 3P_J levels according to the statistical weights.

The results of the solution of the rate equations for ^{12}C and for ^{13}C in terms of the pertinent volume emissivity (j value) ratios are given in Figure 2. In this Figure, we plot j_{1907}/j_{1909} for both pure ^{12}C and pure ^{13}C in addition to j_{1910}/j_{1909} for pure ^{13}C . These ratios are shown vs. the log ($N_e\ \text{cm}^{-3}$) for two values of T_e , 10000 and 15000 K. This is a typical range for T_e in PNs and demonstrates that there is minimal dependence on T_e .

Besides the graphical representation shown in Figure 2, it is useful to solve the 4-level rate equations explicitly in the low- N_e limit in terms of algebraic expressions for the atomic data. As will be seen, this provides superior insight when we compare the observed line ratios with theoretical predictions. The expression for the familiar N_e -diagnostic line ratio may be written,

$$\frac{I(1907)}{I(1909)} = \frac{N_4 A_{41} \nu_{41}}{N_3 A_{31} \nu_{31}} . \quad (1)$$

Here we need to obtain N_4/N_3 . How this was done for the general 3-level atom rate equations may be seen from equations 2 and 3 in Rubin (1986). Because we are writing the equations for just the low- N_e limit, when $A_{21} \neq 0$, all the terms arising from levels above ground that contain the square of the density are dropped (e.g., collisional routes out are negligible). Also terms with very low A_{ij} may be neglected. Then, in the low- N_e limit when $A_{21} \neq 0$:

$$\frac{I(1907)}{I(1909)} = 1.001 \frac{C_{14} A_{41}}{C_{13} A_{41} + C_{14} A_{43}} , \quad (2)$$

where $C_{ij} = \Upsilon_{ij} \exp(-\chi_{ij}/kT_e)$. The χ s are the energy level differences and k is the Boltzmann constant. Because $A_{43} \ll A_{41}$, then

$$\frac{I(1907)}{I(1909)} = 1.001 \frac{C_{14}}{C_{13}} . \quad (3)$$

Table 2. Effective Collision Strengths and Transition Probabilities for 4-Level C III

i-j	T_e				$A_{ji} \text{ s}^{-1}$
	5000	10000	15000	20000	
1-2 ^a	0.13	0.11222	0.10711	0.10556	0 (for ¹² C) 9.04E-4 (for ¹³ C) ^c
1-3 ^a	0.39	0.33667	0.32133	0.31667	103 ^{d,e}
1-4 ^a	0.65	0.56111	0.53556	0.52778	5.14E-3 ^c
2-3 ^b	0.800	0.950	1.01	1.03	2.39E-7 ^f
2-4 ^b	0.590	0.695	0.797	0.855	1.4E-13 ^c
3-4 ^b	2.23	2.75	3.05	3.23	2.39E-6 ^c

^aDon Griffin (private communication) using Mitnik et al. 2003 partitioning among levels according to statistical weights

^bKeenan et al. 1992

^cBrage et al. 1998

^dDoerfert et al. 1997

^eJönsson & Froese Fischer 1998

^fFleming et al. 1996

When we assume that all $\exp(-\chi_{1j}/kT_e)$ are approximately the same, then

$$\frac{I(1907)}{I(1909)} \sim \frac{\Upsilon_{14}}{\Upsilon_{13}} = \frac{5}{3}, \quad (4)$$

following the ratio of the statistical weights. This is the equation governing the ^{13}C ratio.

In the low- N_e limit when $A_{21} = 0$, the collisional terms arising from level 2 are retained. Thus, in the low- N_e limit when $A_{21} = 0$:

$$\frac{I(1907)}{I(1909)} = 1.001 \frac{C_{12} \Upsilon_{24} + C_{14} (\Upsilon_{23} + \Upsilon_{24} + \Upsilon_{12})}{C_{12} \Upsilon_{23} + C_{13} (\Upsilon_{23} + \Upsilon_{24} + \Upsilon_{12})}. \quad (5)$$

The last Υ_{12} term arises from collisional deexcitation out of level 2 and the symmetry of Υ_{21} and Υ_{12} . Again, when all $\exp(-\chi_{1j}/kT_e)$ are nearly the same, then

$$\frac{I(1907)}{I(1909)} \sim \frac{\Upsilon_{12} \Upsilon_{24} + \Upsilon_{14} (\Upsilon_{23} + \Upsilon_{24} + \Upsilon_{12})}{\Upsilon_{12} \Upsilon_{23} + \Upsilon_{13} (\Upsilon_{23} + \Upsilon_{24} + \Upsilon_{12})}. \quad (6)$$

This is the equation governing the ^{12}C ratio. We note that the second terms (including the parenthesized values) in the numerator and denominator dominate, and if the first terms were not present, would give the same result 5/3 as the ^{13}C ratio. It is interesting that the two solutions hinge on just A_{21} . Yet it is true that the low- N_e limits for both the ^{12}C and ^{13}C C III ion depend on the collision strengths.

Let us now consider the ratio $I(1910)/I(1909)$ in the low- N_e limit with $A_{21} \neq 0$. This is for the case of pure ^{13}C . The bottom curve in Figure 2 and the behavior in the low- N_e that we are about to work out do not include any contribution from ^{12}C to the main lines. Starting with

$$\frac{I(1910)}{I(1909)} = \frac{N_2 A_{21} \nu_{21}}{N_3 A_{31} \nu_{31}}, \quad (7)$$

we find,

$$\frac{I(1910)}{I(1909)} = 0.9995 \frac{C_{12} A_{41} - C_{14} A_{43}}{C_{13} A_{41} + C_{14} A_{43}}. \quad (8)$$

The comments and assumptions that lead from equation (1) to (2) apply here, except that N_2/N_3 is apropos now. Again, when all $\exp(-\chi_{1j}/kT_e)$ are nearly the same, then

$$\frac{I(1910)}{I(1909)} \sim \frac{\Upsilon_{12} A_{41} - \Upsilon_{14} A_{43}}{\Upsilon_{13} A_{41} + \Upsilon_{14} A_{43}}. \quad (9)$$

The second terms in the numerator and denominator are negligible compared with the first terms; by dropping them, one obtains

$$\frac{I(1910)}{I(1909)} \sim \frac{\Upsilon_{12}}{\Upsilon_{13}} = \frac{1}{3}, \quad (10)$$

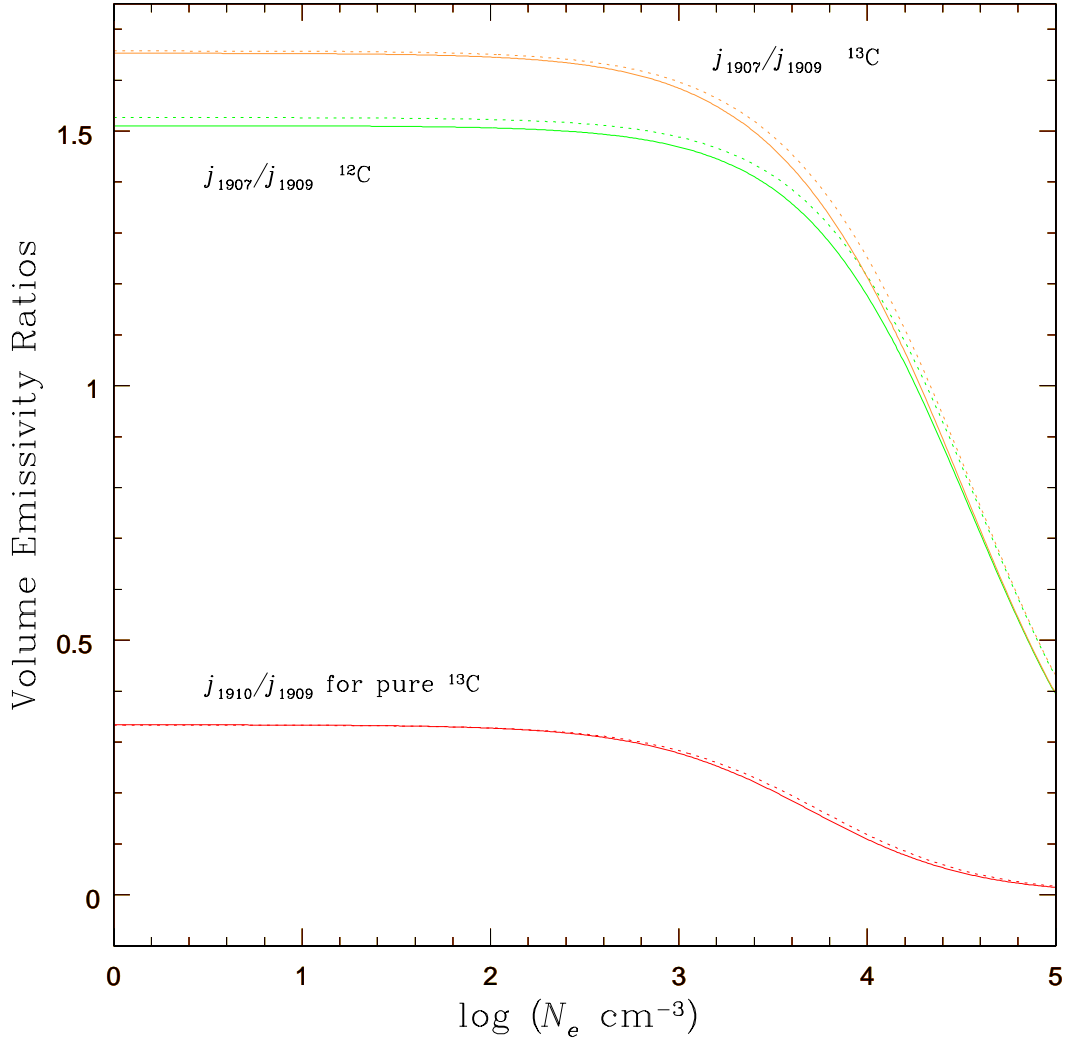


Fig. 2.— The ratio of volume emissivities vs. $\log(N_e \text{ cm}^{-3})$, from top to bottom: j_{1907}/j_{1909} for pure ^{13}C and ^{12}C respectively, j_{1910}/j_{1909} for pure ^{13}C . Note that the j_{1909} values *differ* for the ^{12}C and ^{13}C curves. The solid and dashed lines are for $T_e = 10000$ and 15000 K .

following the ratio of the statistical weights.

The equations derived in this section agree extremely well with the low- N_e limits shown in Fig. 2. The small variations with T_e are also in agreement between the analytical expressions and Fig. 2.

4. Interpretation of the Observed Line Fluxes

It is important to realize that the “main” lines 1907 and 1909 are produced by *both* ^{12}C and ^{13}C . Following Brage et al. (1998), we may write an equation for the intrinsic line ratio $I(1910)/I(1909) = I_{21}/I_{31}$ as

$$\frac{I_{21}}{I_{31}} = \frac{\nu_{21}}{\nu_{31}} \frac{n_2 A_{21}}{(rm_3 + n_3) A_{31}}, \quad (11)$$

where r is the $^{12}\text{C}/^{13}\text{C}$ abundance ratio, n_2 , n_3 , and n_4 are the fractional populations for levels 2, 3, and 4 for ^{13}C and m_3 and m_4 are the fractional populations for levels 3 and 4 for ^{12}C . That is the sum over n_i , $i = 1-4$ is unity, as is the sum over m_i . Values of n_i and m_i are determined from solving the respective rate equations.

We also write an analogous equation for the ratio of the main lines $I(1907)/I(1909) = I_{41}/I_{31}$ as

$$\frac{I_{41}}{I_{31}} = \frac{\nu_{41}}{\nu_{31}} \frac{(rm_4 + n_4) A_{41}}{(rm_3 + n_3) A_{31}}. \quad (12)$$

For each of the sources in Table 1, there are measured flux ratios for $F(1907)/F(1909)$. In addition, an upper limit to $F(1910)/F(1909)$ may be set by using 3σ as the upper limit for the non-detected 1910 Å lines. (Because lines in this multiplet are so close together, intrinsic flux ratios are equivalent to observed flux ratios.)

Equations (11) and (12) are two relations that depend on r and N_e with only a weak dependence on T_e . For the solution of these equations, we use $T_e = 10000$ K. An iterative solution converged rapidly with the results for $N_e \text{ cm}^{-3}$ and r , the $^{12}\text{C}/^{13}\text{C}$ abundance ratio, entered in the last two columns of Table 1. Just as rapidly, there is an indication when there is no possible solution. For these cases, a dash is shown in the $^{12}\text{C}/^{13}\text{C}$ -column with the N_e value found assuming pure ^{12}C . The reason that a range in N_e is shown for those PNs with a lower limit for $^{12}\text{C}/^{13}\text{C}$ is that the higher number for N_e corresponds to the solution of equations (11) and (12) for that limiting value of r . This value of N_e is in fact an upper limit to the actual N_e , which may range down to the smaller number shown for pure ^{12}C .

4.1. The Flux Ratio F(1907)/F(1909)

For some of the PNs, we found that the measured 1907/1909 Å flux ratio was higher than the theoretical low- N_e limit for ^{12}C 1.511, 1.526, and 1.537 at T_e 10000, 15000, and 20000 K, respectively. For instance NGC 6818 has $F(1907)/F(1909) = 1.73$, significantly higher than the atomic data predict. Rubin et al. (2001) found a similar problem for other N_e -diagnostic line ratios. In the most recent work, Rubin (2003) found that the observed [Ne V] 14.3/24.3 μm flux ratio was out of theoretical bounds on the low- N_e limit for 10 out of 20 PNs in the Infrared Space Observatory (ISO) archive, including NGC 6818.

A mixture of ^{13}C with ^{12}C helps to close the gap somewhat. The theoretical low- N_e limit for ^{13}C is 1.653, 1.658, and 1.660 at T_e 10000, 15000, and 20000 K, respectively. However, even if half the carbon were ^{13}C , observed $F(1907)/F(1909)$ ratios as high as 1.73 would not be explained. Indeed any ratio exceeding the 5/3 value would not comport with present predictions. The value of 5/3 is the result of the standard practice of partitioning the 1S_0 - 3P_J multiplet value among the fine-structure levels according to the statistical weights (1, 3, 5). Consequently, this 5/3 limit does not depend on whose set of collision strengths is employed as long as they are partitioned in this way. An observational program to measure very accurate $F(1907)/F(1909)$ ratios would be most useful. On the theoretical side, a detailed calculation for the effective collision strengths between these individual LS levels would be extremely valuable.

4.2. The Flux Ratio F(1910)/F(1909)– Detection of the ^{13}C line in NGC 2440

The IUE data and analysis presented in Table 1 show only one source, NGC 2440, with a significant detection of the ^{13}C line (Figure 3). This is the coadded spectrum of two archival spectra SWP 7263 and LWR 10741. The apertures for both spectra were centered at the same position. The position angles of the aperture major axis were 199.19 and 20.32° respectively (only $\sim 1^\circ$ mismatch) thus providing nearly the same sky coverage. Exposure times were 3600 s on 1979 November 29 and 16200 s on 1981 May 29 respectively and were observed under programs NCBJH and NPDJH, PI J. Patrick Harrington.

In the coadded spectrum the observed flux of the 1909.6 Å line is $(5.94 \pm 1.47) \times 10^{-13}$ erg cm^{-2} s^{-1} , which is a 4σ detection. The simultaneous solution of equations (11) and (12), assuming $T_e = 10000$ K, gives $N_e = 2460 \text{ cm}^{-3}$ and $^{12}\text{C}/^{13}\text{C} = 4.4$. With an assumed T_e of 15000 K, the solution becomes $N_e = 3130 \text{ cm}^{-3}$ and $^{12}\text{C}/^{13}\text{C} = 4.2$. We prefer the former solution because according to figure 2 (T_e vs. I.P.) in Bernard Salas et al. (2002), it appears that the T_e value for the C^{++} zone in NGC 2440 is closer to 10000 than 15000 K for the case

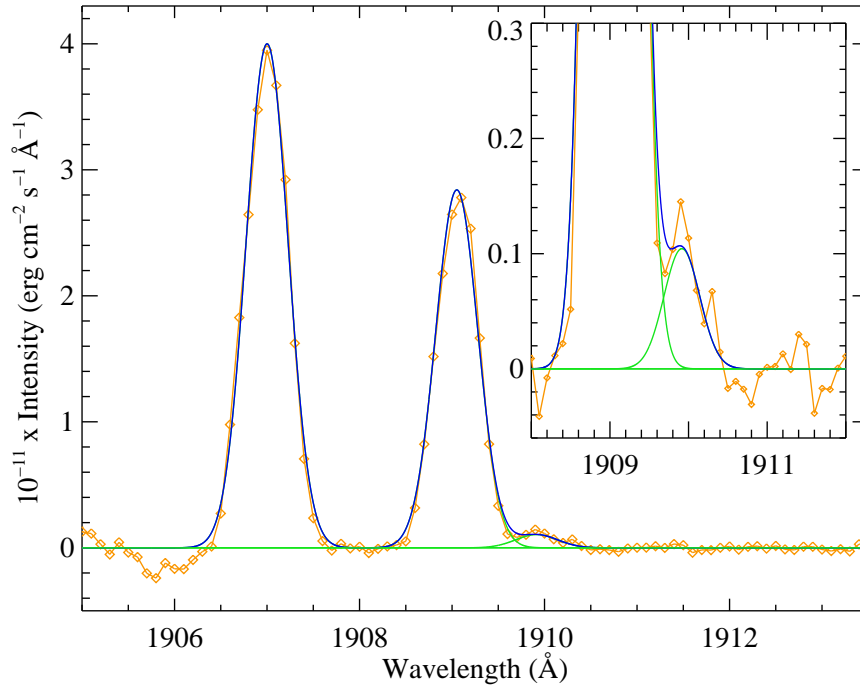


Fig. 3.— Spectrum in the vicinity of the C III multiplet for NGC 2440 resulting from the coaddition of IUE high dispersion, large aperture spectra SWP 7263 and LWR 10741. The continuum is very weak compared with the 1907 and 1909 Å lines and has been fit with a quadratic baseline and removed. The inset shows a magnified (in intensity) view of the ^{13}C 1910 Å line. The 3-component Gaussian fit (see text) and sum are shown, as well as the line connecting the data points (diamonds).

$C^+ \rightarrow C^{++}$ with ionization potential (I.P.) 24.4 eV. Although not sensitive to the assumed T_e , the general trend we find here is that the higher the T_e , the higher the derived N_e and the lower the derived $^{12}C/^{13}C$. We estimate the uncertainty in the value of $^{12}C/^{13}C$ as ± 1.2 from separate measurements and analysis of the two individual IUE spectra.

In their study of NGC 2440, Bernard Salas et al. used these same two IUE spectra. According to their table 3, $F(1907) = 2.43 \times 10^{-11}$ and $F(1909) = 1.77 \times 10^{-11}$ erg cm $^{-2}$ s $^{-1}$. This leads to $F(1907)/F(1909) = 1.373$, while they have a slightly different ratio of 1.35 in their table 5 where they also list the derived $N_e = 4360$ cm $^{-3}$ assuming $T_e = 15000$ K. We compare these to our entries in Table 1: $F(1907) = 2.24 \times 10^{-11}$ and $F(1909) = 1.57 \times 10^{-11}$ erg cm $^{-2}$ s $^{-1}$. This leads to $F(1907)/F(1909) = 1.427$, which will result in a lower derived N_e irrespective of accounting for the effect of the presence of ^{13}C . It is not clear why their line fluxes are higher than ours. It may be due to several factors. For instance, they may have used the pre-NEWSIPS calibration. They likely used a different technique than ours to form a weighted average of the two IUE spectra. Their fluxes may be taken directly from the Gaussian-fit areas whereas we have used Gaussian fits for guidance but use the option in ISAP [moment fit] and IRAF [splot e-option] to measure the areas (except for measuring the 1910 line with the Gaussian). Generally we find that departures from a Gaussian profile result in somewhat smaller line fluxes. Additionally, the fitting of lines is not totally objective, e.g, in the manner of accounting for the baseline, etc.

Although the line was not detected in any of the other PNs, we were able to establish lower limits for the $^{12}C/^{13}C$ ratio for many. Even when coadding many spectra, the S/N was not high enough to ascertain a useful value of $^{12}C/^{13}C$ for most objects. HST studies similar to those of Palla et al. (2002) and Clegg et al. (1997) could be used to refine the limits presented here.

At a late stage in our work on this project, we were surprised to discover that a similar project had been undertaken by Miskey et al. (2000). They report a detection in NGC 2440, but appear to derive a much higher $^{12}C/^{13}C$ ratio of 39. They also report a detection in NGC 6302 with a ratio of 23. Unfortunately, since only an AAS abstract has been published, their data and methods are not available for scrutiny. We cannot report a detection of the 1910 Å line in NGC 6302. Two short wavelength spectra (SWP 10391 and SWP 8971) and one long wavelength spectrum (LWR 7722) are available for this nebula. Even the 1907, 1909 main lines are indistinguishable from the noise in LWR 7722; coadding SWP 10391 and SWP 8971 produces a non-detection of the 1910 line. SWP 10391 shows a small peak at the correct location, but at the same level as the noise; thus a detection cannot be conclusively claimed.

While ten SWP and eight LWP/LWR spectra were available for NGC 3918, many of

them showed saturation in the strong C III lines, making them unusable for determining ratios. Similarly, all four available SWP spectra for NGC 3242 are saturated, and the values from Table 1 come from only LWR 12705. Our limits are consistent with the findings of Clegg et al. (1997) and Palla et al. (2002). We note that Palla et al. used a 1σ upper limit for F(1910), while we use 3σ . Using their 1σ value and main line fluxes for NGC 3242 with our improved atomic data here, we find that their $^{12}\text{C}/^{13}\text{C} \geq 38$ becomes ≥ 44.4 . However, when we use a 3σ observed upper limit from their paper, then more conservatively $^{12}\text{C}/^{13}\text{C} \geq 14$, a value very similar to our limit in Table 1.

5. Discussion and Conclusions

NGC 2440 has an unusually massive central star (CS), $0.72 M_{\odot}$, according to Wolff et al. (2000), and $0.932 M_{\odot}$, according to Górny et al. (1997). The progenitor star is believed to be more massive than $4 M_{\odot}$, e.g., figure 3 in Balser et al. (2002) has $\sim 4.2\text{--}4.3 M_{\odot}$ (see also the discussion in their §2). In their study of NGC 2440, Bernard Salas et al. (2002) concluded, based on a measured $(\text{C+N+O})/\text{H}$ ratio higher than that for NGC 7027, that the CS must have been a more massive progenitor than was the star in NGC 7027, for which Bernard Salas et al. (2001) found $3\text{--}4 M_{\odot}$. Above $4 M_{\odot}$, asymptotic giant branch (AGB) stars develop deep convective envelopes with very high base temperatures, leading to the operation of the CN-cycle; hence the name, hot bottom burning. There, the CN-cycle operates at the base of the convective envelope in a hydrogen-burning shell, where ^{12}C is converted into ^{13}C and then into ^{14}N . This process would tend to drive $^{12}\text{C}/^{13}\text{C}$ toward the CN-cycle equilibrium ratio of ~ 3.3 (Smith & Lambert 1990; Frost et al. 1998). When ratios close to the CN-cycle equilibrium value are measured in a star’s atmosphere, it is indicative of the presence of nearly pure CN-cycle material. Thus, the low $^{12}\text{C}/^{13}\text{C}$ ratio of 4.4 ± 1.2 that we find for NGC 2440 does support this picture.

If the progenitor were less massive than $4 M_{\odot}$, then the scenario changes. Both the cool bottom processing (CBP) and standard models predict $^{12}\text{C}/^{13}\text{C} \simeq 20\text{--}30$ for stars between $3\text{--}4 M_{\odot}$ (Boothroyd & Sackmann 1999; Renzini & Voli 1981). Then our derived $^{12}\text{C}/^{13}\text{C}$ for NGC 2440 would not appear to support either the standard or CBP theories. While CBP does produce ratios as low as 4.4, it is only expected to occur in progenitor stars of $\leq 2 M_{\odot}$ (Wasserburg et al. 1995). Two (unlikely) possibilities might allow agreement. First, were the mass estimates for the CS progenitor too large by a factor of ~ 2 , our $^{12}\text{C}/^{13}\text{C} = 4.4$ for NGC 2440 would support the CBP theory. Second, perhaps CBP occurs in stars of $3\text{--}4 M_{\odot}$. This is in fact contrary to the statement by Wasserburg et al. (1995) that no CBP is expected above $\sim 2.3 M_{\odot}$. However a reconsideration of model parameters might be useful

to determine whether this could occur.

The small $^{12}\text{C}/^{13}\text{C}$ we find for NGC 2440 is in the range derived by Balser et al. (2002) in their study of molecular clouds associated with PNs. As mentioned in the Introduction, from observations of ^{12}CO and ^{13}CO millimeter lines, they found values of $^{12}\text{C}/^{13}\text{C}$ from 2.2–31 in 9 PNs. The extreme low value 2.2 ± 0.03 was for the bipolar PN M1–16, which is not on our list. We note that our small ratio for NGC 2440 is consistent with measurements of J-type carbon stars. Abia & Isern (1997) found $\langle^{12}\text{C}/^{13}\text{C}\rangle = 6\pm 3$ while Ohnaka & Tsuji (1999) in their analysis of 26 J-type C stars found an even lower average of 4.7 ± 2.8 with several ratios as low as ~ 1 –2, well below the equilibrium value for the CN-cycle.

The question remains as to why NGC 2440 is the only nebula among those we measured which has a detectable 1909.6 \AA ^{13}C hyperfine structure line, as well as why it has such a low $^{12}\text{C}/^{13}\text{C}$. Using IUE archival data, we also set upper limits on F(1909.6) in 40 other PNs available and lower limits for $^{12}\text{C}/^{13}\text{C}$ in 23 of these. IUE had limited dynamic range that precludes setting more stringent limits for most objects, though coadding spectra allows better S/N. NGC 2440 is among the brightest PNs in terms of either of the main line fluxes; only NGC 2867, NGC 3242, NGC 3918, and NGC 7662 are higher (see Table 1). By using the measured 3σ as an upper limit to their F(1909.6), we derive lower limits on $^{12}\text{C}/^{13}\text{C}$ for these four nebulae of respectively 5.9, 14.5, 9.9, and 6.5 – already higher than what we find for 2440. NGC 2440 is carbon rich with C/O of 1.9 (Bernard Salas et al. 2002) and a high excitation Peimbert type I PN (Hyung & Aller 1998), that is, it is a N- and He-rich PN. The central star is among the hottest ($\sim 200,000$ K) and most massive known (see earlier discussion). In fact, in their entire sample of ~ 80 PNs, Górný et al. (1997) derived a CS mass of $0.932 M_{\odot}$, which was the second largest of all. This nebula also has T_e reaching as high as 15000 – 20000 K as measured in several high ionization species (Bernard Salas et al. 2002). NGC 2440 has a relatively low N_e of 2460 cm^{-3} determined here (see Table 1). Both lower N_e and lower $^{12}\text{C}/^{13}\text{C}$ lead to a higher F(1910)/F(1909). It may be that Type I PNs have lower $^{12}\text{C}/^{13}\text{C}$ ratios. Furthermore, NGC 2440 is a bipolar PN. In their study, Balser et al. (2002) found those PNs that have the lowest values of $^{12}\text{C}/^{13}\text{C}$ are classified as bipolar. Further theoretical and observational work is needed to determine the cause of the low ratios. An HST spectroscopic study of the C III multiplet in NGC 2440 would be desirable.

Several of the PNs have the measured F(1907)/F(1909) outside the low- N_e theoretical limit for ^{12}C . Uncertainties in the measured fluxes may account for some of these differences. A mixture of ^{13}C with ^{12}C helps narrow the gap somewhat. Nevertheless, some of observed F(1907)/F(1909) ratios still appear too high to conform to the presently predicted limits. We have shown that both the F(1907)/F(1909) and the F(1910)/F(1909) ratios in the low- N_e

limit are predominantly influenced by using the standard partitioning among the collision strengths for the multiplet $^1S_0-^3P_J$ according to the statistical weights. A detailed calculation for the effective collision strengths between these individual levels would be valuable. The determination of reliable N_e values by this method as well as the $^{12}\text{C}/^{13}\text{C}$ abundance ratio depends on it. As far as we know, it appears that there have been no previous attempts to account for the presence and effects of ^{13}C when using the well-known C III N_e -diagnostic F(1907)/F(1909).

Support for this work from a NASA Astrophysics Data Program (ADP) grant NAG5-13030 is gratefully acknowledged. We thank the NASA Undergraduate Research Program (NASA-USRP), which made 2003 summer work for EEC at NASA/Ames possible. Valuable contributions were made by David Ho and Alessandra Radicati. Thanks to Janet Simpson and Mónica Rodríguez for reading the paper and helpful remarks. We thank Myron Smith and Randy Thompson for providing useful comments on various aspects of the IUE spectra. RHR acknowledges support from the Long-Term Space Astrophysics (LTSA) program and thanks Scott McNealy for providing a Sun workstation.

REFERENCES

- Abia, C., & Isern, J. 1997, MNRAS, 289, L11
- Balser, D.S., McMullin, J.P., & Wilson, T.L. 2002, ApJ, 572, 326
- Bernard Salas, J. B., Pottasch, S. R., Beintema, D. A., & Wesselius, P. R. 2001, A&A, 367, 949
- Bernard Salas, J. B., Pottasch, S. R., Feibelman, W. A., & Wesselius, P. R. 2002, A&A, 387, 301
- Boothroyd, A. I., & Sackmann, I.-J. 1999, ApJ, 510, 232
- Brage, T., Judge, P.G., Aboussaid, A., Godefroid, M.R., Joensson, P., Ynnerman, A., Fischer, C.F., & Leckrone, D.S. 1998, ApJ, 500, 507
- Charbonnel, C., & do Nascimento, J. D. 1998, A&A, 336, 915
- Clegg, R.E.S. 1985, in Danziger, I.J., Matteucci, F., Kj ar, K., eds, ESO Workshop on Production and Distribution of C, N, O Elements. ESO, Garching, p. 261
- Clegg, R.E.S., Storey, P.J., Walsh, J.R., & Neale, L. 1997, MNRAS, 284, 348

- Doerfert, J., Träbert, E., Wolf, A., Schwalm, D., & Uwira, O. 1997, *PhRvL.*, 78, 4355
- Fleming, J., Bell, K.L., Hibbert, A., Vaeck, N., & Godefroid, M.R. 1996, *MNRAS*, 279, 1289
- Frost, C.A., Cannon, R.C., Lattanzio, J.C., Wood, P.R., & Forestini, M. 1998, *A&A*, 332, L17
- Górny, S.K., Stasińska, G., & Tylenda, R. 1997, *A&A*, 318, 256
- Hyung, S., & Aller, L.H. 1998, *PASP*, 110, 466
- Jönsson, P., & Froese Fischer, C. 1998, *Phys.Rev.A*, 57, 4967
- Keenan, F.P., Feibelman, W.A., & Berrington, K.A. 1992, *ApJ*, 389, 443
- Miskey, C. L., Feibelman, W. A., & Bruhweiler, F. C. 2000, *AAS Abstract*, 196, 43.04
- Mitnik, D.M., Griffin, D.C., Ballance, C.P., & Badnell, N.R. 2003, *JPhB*, 36, 717
- Ohnaka, K., & Tsuji, T. 1999, *A&A*, 345, 233
- Palla, F., Bachiller, R., Stanghellini, L., Tosi, M., & Galli, D. 2000, *A&A*, 355, 69
- Palla, F., Galli, D., Marconi, A., Stanghellini, L., & Tosi, M. 2002 *ApJ*, 568, L57
- Renzini, A., & Voli, M. 1981, *A&A*, 94, 175
- Rubin, R.H. 1986, *ApJ*, 309, 334
- Rubin, R.H. 2003, in *IAU Symp. 217, Recycling Intergalactic and Interstellar Matter*, ASP Conference series, Eds. P.-A. Duc, J. Braine, & E. Brinks (in press)
- Rubin, R.H., Dufour, R.J., Geballe, T.R., Colgan, S.W.J., Harrington, J.P., Lord, S.D, Liao, A.L., & Levine, D.A. 2001, in *Spectroscopic Challenges of Photoionized Plasmas*, ASP Conference series, Vol. 247, 2001, Eds. G.J. Ferland & D.W. Savin, p. 479, “Infrared Spectroscopy of Atomic Lines in Gaseous Nebulae”, ([astro-ph/0109398](#))
- Sackmann, I.-J., & Boothroyd, A. I. 1999, *ApJ*, 510, 232
- Smith, V.V., & Lambert, D.L. 1990, *ApJS*, 72, 387
- Wasserburg, G.J., Boothroyd, A.I., & Sackmann, I.-J. 1995, *ApJ*, 447, L37
- Wolff, M. J., Code, A. D., & Groth, E. J. 2000, *ApJ*, 119, 302